International Global Navigation Satellite Systems Society
IGNSS Symposium 2007

The University of New South Wales, Sydney, Australia
4 – 6 December, 2007

Statistic analysis of daily position time series from the Hong Kong local dense GPS network

Linguo YUAN, Xiaoli DING, Wu CHEN
Department of Land Surveying and Geo-informatics, The Hong Kong Polytechnic University, Hong Kong, China
Tel. + 852 2766 5965, Fax. +852 2330 2994, E-mail: lsxlding@polyu.edu.hk
Simon KWOK, Raymond CHAN
Geodetic Survey Section, Lands Department, Hong Kong SAR, China

ABSTRACT

Continuous GPS observations of 12 GPS stations from January, 2001 to August, 2007 in the Hong Kong local dense GPS network are processed to obtain reliable coordinates and velocities of the stations in the ITRF2005. A spatial filtering algorithm using the principal component analysis is employed to remove the common mode errors from the daily position time series. The noise characteristics of the filtered position time series are assessed using the method of maximum likelihood estimation. The results indicate that spatially correlated common mode errors are a dominant error source in the daily GPS solutions and that there are strong seasonal signals in all the three coordinate components. The higher-order ionospheric effects are a limiting factor on the accuracy of the station coordinates in our study area. The noise in the filtered position time series can be described as a combination of variable white noise plus flicker noise. The velocity uncertainties are about 2-6 times larger if only variable white noise is assumed. The maximum relative horizontal velocity between the sites is on the order of 2 mm/yr, which indicates some local fault activities. In addition, there are obvious local seasonal signals in the filtered position time series. The local annual amplitudes are up to 1.5 mm for the horizontal components and 2.2 mm for the vertical components. The residual scatters of the filtered time series also show strong seasonal characteristics.

KEYWORDS: GPS, time series, spatial filtering, seasonal signals

1. INTRODUCTION

The rapid increasing worldwide Continuous Global Positioning System (CGPS) networks under the umbrella of the International GNSS Service (IGS) have been widely used over the last decade for a variety of geophysical studies from global to regional and local scales, such as global plate motion (e.g., Kreemer *et at.*, 2003; Prawirodirdjo and Bock, 2004), surface loading deformation (e.g., Dong *et al.*, 2002), regional crustal deformation (e.g., Zhang, 1996; Lidberg *et al.*, 2007), and local fault activity (e.g., Hill and Blewitt, 2006). The progress in these studies has led to an increasing demand for more precise position time series. Correspondingly, many studies have been devoted to the evaluation and elimination of various sources of noise in GPS time series analysis in order to extract more information from the position time series.

The Hong Kong Satellite Positioning Reference Station Network (SatRef) was commenced to establish by the Lands Department of Hong Kong SAR government since 2000, with a primary goal to develop an active navigation and positioning infrastructural service system for Hong Kong. The project implementation was carried out in two phases. The Phase I was implemented in 2000 with six GPS Permanent Reference Stations constructed in the northwest and northern part of the Hong Kong Territory. To extend the network coverage, the Phase II for the establishment of another six stations in the Lantau Island, Hong Kong Island and eastern part of the territory was established in early 2004. Up to now, the network consists of 12 Continuously Operating Reference Stations evenly distributed in Hong Kong, with a station spacing of about 10 km to 15 km. The location of the SatRef stations is shown in Figure 1. Further information about SatRef stations may refer to the SatRef web page (http://www.geodetic.gov.hk/smo/index.htm).

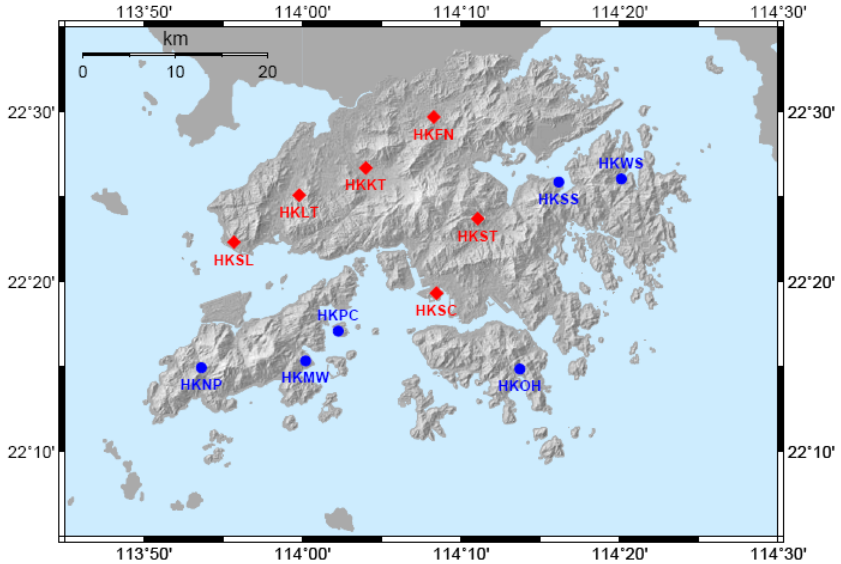

Figure 1. Distribution of the Hong Kong GPS reference stations. Stations established in 2000 are marked with diamonds, while stations established in 2004 are shown as dots.

This paper concentrates on statistic analysis of daily position time series of the Hong Kong permanent stations in order to obtain reliable and accurate station coordinates and velocities in the ITRF2005. A spatial filtering algorithm using the principal component analysis is employed to remove the common mode signatures from the daily position time series. The noise characteristics of the filtered time series is assessed using the method of maximum

likelihood estimation (MLE). Special attention is given to the seasonal features in the position time series.

2. DATA ANALYSIS

2.1 GPS Data Analysis

In this study, we have analysed SatRef GPS observations of the Phase I from January 2001 until August 2007, and GPS observations of the Phase II from June 2004 until December 2006. The daily site coordinates were estimated from GPS observations using the GAMIT/GLOBK software packages, version 10.3(Herring et al., 2006a, 2006b) in three main steps and adopting a distributed processing strategy described by Zhang (1996).

In the first step, double-difference phase and code observations from each day were processed with GAMIT software to estimate station coordinates, satellite orbits, earth orientation parameters (EOP), and two-hourly piecewise-linear atmospheric zenith delay together with daily gradient parameters. Phase ambiguities were resolved as far as possible. The elevation cutoff was set to 10°, and the elevation angle dependent weighting of the phase observations were assigned individually for each station based on the preliminary solution. Data were cleaned using 30 second sample rate, and then decimated to the 2 minute rate for the final solution. The IGS absolute elevation dependent antenna models, SIO final orbits, and IERS bulletin B values for EOP were used. The priori zenith hydrostatic delays computed from the empirical Global Pressure and Temperature (GPT) model (Boehm1 *et al.*, 2007) and the Global Mapping Function (Boehm1 *et al.*, 2006) were used. The IERS2003 solid-earth tide and pole tide model (McCarthy and Petit， 2004) and FES2004 ocean tide loading were applied. The parameter estimates and their covariance matrices were output as loosely constrained solutions. We included in this analysis nearby 10 IGS stations (PIMO, KUNM, WUHN, NTUS, LHAS, BJFS, SUWN, DAEJ, SHAO and GUAM) with positions and velocities well determined in the ITRF2005 (Altamimi *et al.*, 2007) to serve as linking our local network and the global IGS network.

In the second step we combined our loosely constrained solutions with the SIO global solutions using GLOBK software. In this step both orbital and common station parameters have been estimated and removed from forward analysis since the orbital and other common information have been incorporated into the estimates and covariances of the station coordinates. Finally, internal constraints were applied by using a set of globally-distributed fiducial station coordinates (see Appendix C of Dong *et al.*, 1998) to define a reference frame for our daily station coordinate estimates.

The basis of the global reference frame is the horizontal coordinates and velocities of the 131 IGS05 Reference Frame sites (http://igscb.jpl.nasa.gov/network/refframe.html) in the ITRF2005. There is no consensus on whether a scale factor is included in the stabilization presently. Here we followed the suggestion described by Lidberg *et al.* (2007) and a seven-parameter transformation (three network rotations, three network translations and one scale factor) has been applied. The GLOBK stabilization automatically eliminated stations from the reference station list whose positions do not agree well with the a priori reference frame. Five iterations were used to eliminate bad sites and to compute station weights for the reference frame stabilization. The site relative weight parameter was set to 0.9, so that 90% of the relative site weights were determined by the coordinate uncertainties from the previous

iteration. Sites with root-sum-square (RMS) of the residuals greater than 4 times the relative weight times the overall root-mean-square of the fit were excluded from the reference frame.

2.2 Spatial Filtering

The resulting raw position time series of the local network contain both signal and noise with strongly spatial correlation. The relatively large common mode signature can mask the small local environmental effects for our small area, and also influence the site velocity and its uncertainty estimation. It is standard practice to filter out the so-called common mode errors (CME) using the regional filtering approach (Wdowinski *et al.*, 1997; Nikolaidis, 2002) in order to increase their signal-to-noise ratio of coordinate time series for the regional GPS network. Dong *et al.* (2006) developed a more general spatiotemporal filtering approach using principal component analysis (PCA) and Karhunen-Loeve expansion (KLE). Here we modified the approach of Dong *et al.* (2006) and adopted the principal component analysis to perform spatial filtering for our local network. The main difference is that we firstly only removed the best-fit model with terms for constant episodic offsets, linear trends and did not remove seasonal (annual and semiannual) terms, since we expect that these annual and semiannual fluctuations may also constitute common mode bias for our small area. Additionally, we adopted an iterative processing method in order to perform the spatial filtering in a more precise manner.

As presented by Dong *et al.* (2006), each component (north, east, and vertical) of the regional or local network daily station position time series $X(t_i, x_j)$ ($i = 1, 2, ..., m$ and $j = 1, 2, ..., n$; m is the spanning days and n is the number of stations) can be decomposed in terms of the spatial eigenvectors and their corresponding temporal amplitudes using the PCA approach

$$X(t_i, x_j) = \sum_{k=1}^{n} a_k(t_i) v_k(x_j) \tag{1}$$

Where $a_k(t)$ is the temporal amplitude of the kth principal component (PC), and $v_k(x)$ is its corresponding eigenvector. Usually the eigenvectors are arranged in the descending order so that the leading few PCs can account for the common mode signature of the entire network, while the higher-order PCs are related to local environmental effects.

The leading three PC spatial eigenvectors of the north, east and vertical components resulting from the PCA decomposition are shown in Figure 2. The first PC eigenvectors have a rather homogeneous spatial pattern. It describes the common mode variations of the entire network and accounts for 93.9%, 94.2%, and 84.6% of the total eigenvalues for the north, east, and vertical components, respectively. The second PC eigenvectors only account for 0.9%, 1.0%, and 2.5% of the total eigenvalues, and the third PC eigenvectors account for 0.9%, 0.9%, and 2.1% of the total eigenvalues for the north, east and vertical components, respectively. The second and third PC eignvectors present the inconsistent patterns through our local network, which suggest that they represent site-dependent phenomena.

Since only the first principal components of the detrended time series explain the common mode variations through our network and their engenvetors have a rather homogeneous spatial pattern, we treat the first PC as CME. The CME from PCA is defined by

$$\varepsilon_i(t_i) = a_1(t_i) \sum_{k=1}^{n} v_k(x_j) / n \tag{2}$$

To sum up, the spatial filtering algorithm consists of the following steps iteratively for the north, east, and vertical components, respectively:

1. Remove the episodic offsets, linear trends from the raw time series by weighted linear regression.
2. Calculate the CME from the residual time series using PCA and remove linear trend from CME.
3. Remove the corresponding CME from the each raw time series. The resulting time series are referred to the filtered time series.
4. Estimate offsets and linear trend terms from the filtered time series and remove the estimated offsets and linear trend terms from the raw time series.
5. Repeat step 2 through 4 until the CME is convergent. In practice, four iterations are enough.

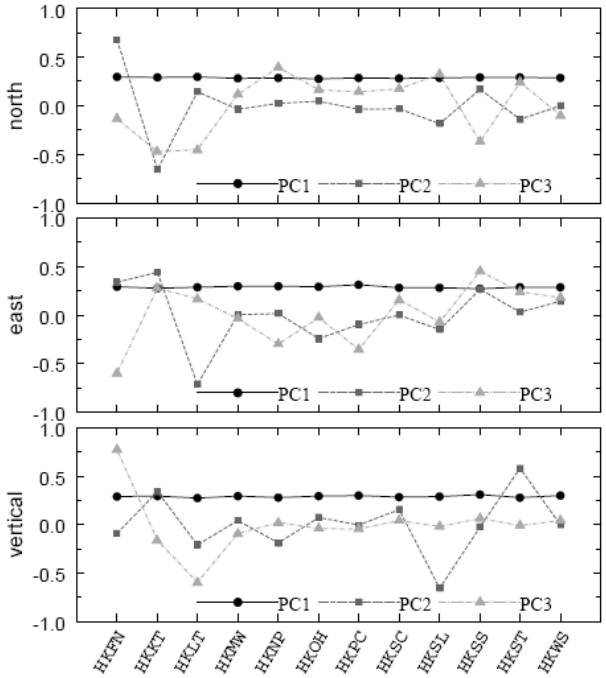

Figure 2. The three leading PC spatial eigenvectors of the north, east, and vertical components resulting from the PCA decomposition.

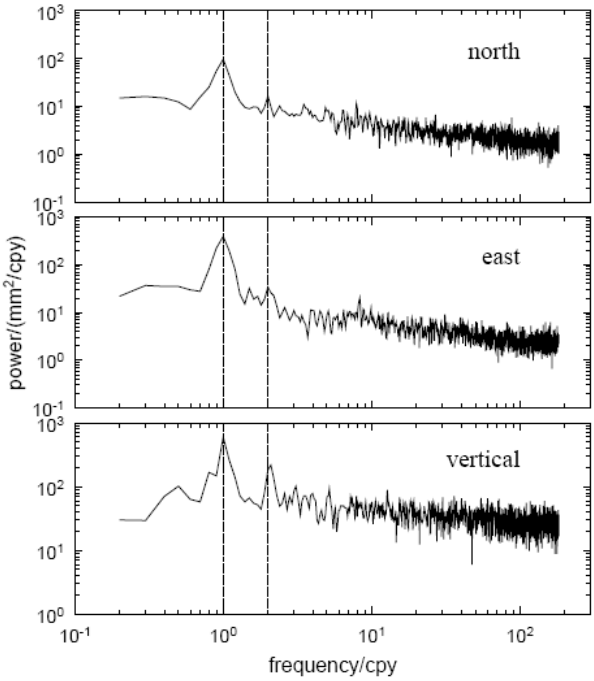

Figure 3. Stacked power spectra of the daily filtered position time series. Vertical dashed lines indicate frequencies of 1.0 and 2.0 cycles per year (cpy).

The filtered time series derived by the above spatial filtering algorithm have removed CME and outliers, but retain their original linear trends and offsets. The application of the spatial filtering algorithm greatly reduces the scatter of postfit residuals by average factors of 2.8, 3.4 and 2.1 for north, east and vertical components, respectively. The average weighted root-mean-square (WRMS) of the raw daily position time series (step 1) are 2.77 ± 0.36 mm (north), 3.91 ± 0.24 mm (east) and 7.17 ± 0.65 mm (up), while the average WRMS of the filtered daily position time series (after step 5) are 0.99 ± 0.13 mm (north), 1.15 ± 0.20 mm (east) and 3.37 ± 0.30 mm (up).

2.3 Position Time Series Analysis

To fit the filtered time series, a time-dependent model with a linear trend, episodic offsets, and periodic components has been used. This model is described by the following

mathematical expression (e.g., Langbein, 2004):

$$d_i = a + bt_i + \sum_{j=1}^{j_0} o_j H(t_i - T_j) + \sum_{m=1}^{m_0} c_m \sin(2\pi f_m t_i + \varphi_m) + v_i \qquad (3)$$

Where a is the site position; b is the linear rate; $H(t_i - T_j)$ is the Heaviside step function; o_j are offsets in the time series at $t_i = T_j$; c_m is amplitude of the each periodic signal at frequency f_m; and v_i denotes noise. For the case of time-independent white noise, we generally apply the weighted least squares to determine the unknown parameters. Several analyses have shown that the GPS position time series contain colored noise (Zhang *et al.*, 1997; Mao *et al.*, 1999; Williams *et al.*, 2004). Neglecting the colored noise may result in underestimation of station velocity uncertainties by a factor of four or more. A common method to handle this problem is to simultaneously estimate the noise structure and the parameters of a time-dependent model of the data using maximum likelihood estimation (e.g. Zhang *et al.*, 1997; Mao *et al.*, 1999; Williams *et al.*, 2004; Langbein, 2004).

In the maximum likelihood formalism, the natural log of the Gaussian probability function is maximized by (e.g. Williams et al., 2004):

$$MLE = \ln[lik(\hat{v}, C)] = -\frac{1}{2}[\ln(\det C) + \hat{v}^T C^{-1} \hat{v} + N \ln(2\pi)] \qquad (4)$$

Where ln is the natural logarithm, N is the number of days, C is the data covariance matrix, and $\hat{v}$ is the postfit residuals from (3) using weighted least squares with the same covariance matrix C. The covariance matrix C can represent many forms of stochastic noise such as white, power-law, first-order Gauss Markov, autoregressive, band pass together with a multitude of combination of the above (e.g. Langbein, 2004; Williams and Willis, 2006). In this paper, we assume the noise that consists of either one or two of the following models: white noise (WH), variable white noise (VW), power-law noise (PL), flicker noise (FN), random walk noise (RW) and first-order Gauss Markov FOGM noise. In total, the 10 models in two groups were tested: WH, FN+WH, RW+WH, PL+WH, GM+WH; VW, FN+VW, RW+VW, PL+VW, GM+VW.

We used spectral analysis to search any potential periodic signals in the filtered time series before the MLE were performed, since neglecting the periodic signals can bias our maximum likelihood estimates (Williams and Willis, 2006). The stacked power spectra using the Lomb-Scargle periodogram method (Press *et al.*, 2001) for the north, east, vertical components, respectively are shown in Figure 3. The annual and semiannual periods are clearly evident in the spectra. In addition, the spectra are not flat (white noise) and their power spectra is higher at low frequency, which indicates the presence of colored noise in the time series. So the annual and semiannual terms are included in the MLE analysis.

3. RESULTS AND DISCUSSION

3.1 Common Mode Errors (CME)

Figure 4 shows the CME time series derived by the above spatial filtering algorithm, and their Lomb-Scargle power spectra are displayed in Figure 5. It can be seen from the results in Figure 5 that the annual and semiannual signals can clearly be seen for the north and vertical components. Furthermore, the semiannual power of the north component is larger than the annual power. However, the annual and semiannual signals for the east component are

relatively obscure and it seems that a three-month period signal exits. The amplitudes and phases of their annual and semiannual signals are estimated using the MLE based on the flicker noise plus white noise model (FN+WH). The solid line in Figure 4 is the fitted time series of the annual and semiannual signals and their estimated amplitudes and phases are given in Table 1.

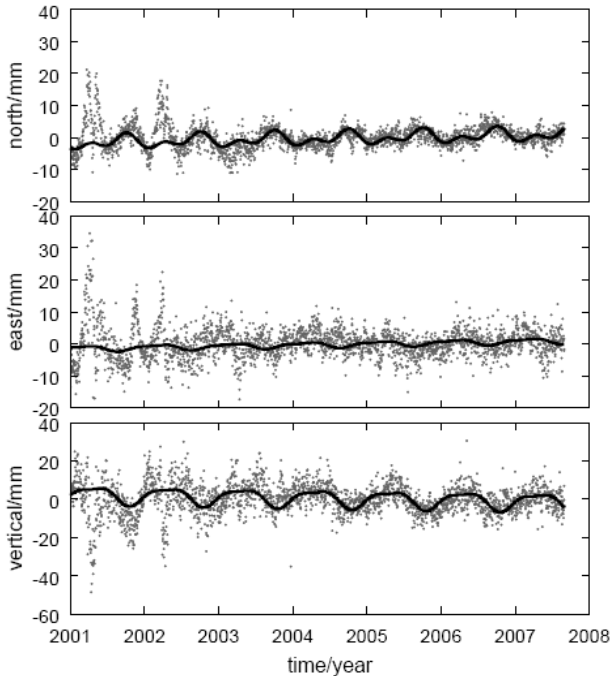

Figure 4. CME time series. The solid line is the fitted time series of annual and semiannual components together with the white noise plus flicker noise model from the MLE.

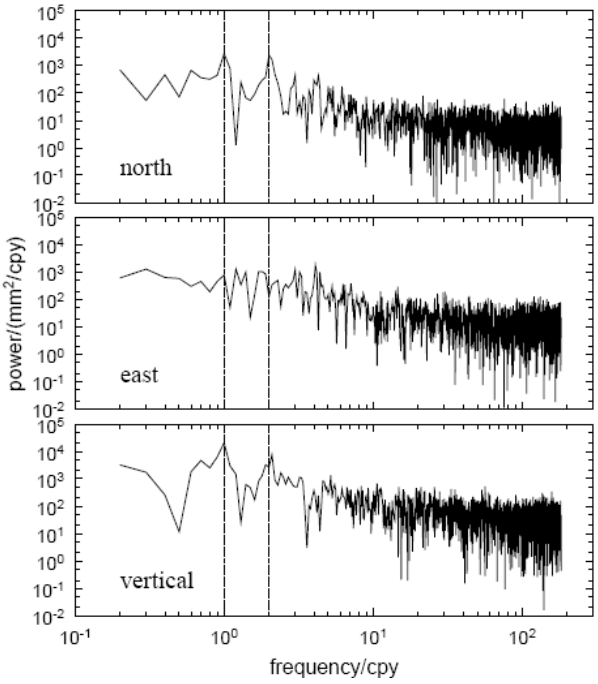

Figure 5. Power spectra of the CME time series. Vertical dashed lines indicate frequencies of 1.0 and 2.0 cycles per year (cpy)

Table 1. Estimated annual and semiannual parameters and their uncertainties (1 σ) of the CME time series based on the flicker noise plus white noise model.

Component	Annual		Semiannual	
	Am(mm)	Ph(°)	Am(mm)	Ph(°)
North	0.89±0.42	217±27	2.10±0.29	258±8
East	1.54±0.60	10±22	0.82±0.43	253±30
Vertical	3.22±1.05	340±18	2.44±0.74	58±17

Phases are referred to January 1. Am = amplitude; ph = phase.

It can be seen from the results in Table 1 that the strong seasonal (annual and semiannual) signals exists in our CME time series. The annual amplitudes are up to 1.5 mm for the horizontal components and 3.2 mm for the vertical components. It must be worthwhile to notice that the north and up components show the strong semiannual variations and their amplitudes are about 2.1 mm and 2.4 mm respectively. Figure 4 indicates that the CME time series are large scatters during the period of 2001 -2003 than the following years. The primary cause for this anomaly is the impact of the higher-order ionospheric terms on the GPS estimates (Kedar *et al.*, 2003; Fritsche *et al.*, 2005; Chen *et al.*, 2007). Chen *et al.* (2007) have shown that the strong ionopheric disturbances in Hong Kong occur frequently during the solar maximum period (2001-2003), particularly around March and September since Hong Kong is located in the magnetic equatorial area. Closer inspection of Figure 4 shows that the positions systematically have the up to 20 mm northward shift tendency of the for the north

components, the up to 40 mm eastward shift tendency for the east components, and the up to 50 mm downward tendency for the up components, respectively during the solar maximum period, which is very consistent with the results of Kedar *et al.* (2003) and Fritsche *et al.* (2005). Furthermore, Kedar *et al.* (2003) has shown that the strong semi-annual north-south oscillation is due to the higher-order GPS ionospheric effects. So we infer that our strong north semiannual variation is also mainly caused by the higher-order ionopheric effects, although other geophysical phenomena (such as nontidal oceanic mass, atmospheric loading and groundwater loading; Dong *et al*., 2002) and spurious long-period signatures (Penna *et al.*, 2007) may also contribute this periodic variation. Whether the higher-order ionospheric effects also contribute to our strong vertical semiannual oscillation (~2mm) and other inter-annual signature need be still further investigated. All in all, the higher-order ionospheric effects are the prominent factor impacting on the GPS coordinates in our studying area.

3.2 Noise Characteristics

With 10 noise models, 12 sites and three components being test, it would be hard to find a simple way to show the results. In general, larger values of the maximum likelihood (ML) indicate the preferred model, where the ML value is the natural logarithm of the likelihood function shown by equation (4). So we attempt to find a single dominant model and show the results for just this model in terms of the largest ML values following the method presented by Williams and Willis (2006). The previous Monte Carlo simulations (Langbein, 2004; Beavan, 2005; Williams and Willis, 2006) indicate that the difference (δ ML) between two models in ML value greater than around 3.0 is significant at the 95% confidence level. For the difference of GM and other models this value may be a little low and Williams and Willis (2006) suggests a value of around 4.7 for the difference of the GM and FN model. The average δ ML between the ML for the white noise only model and other 9 models is shown in Figure 6 for the north, east and vertical components of all 12 sites, respectively.

It can be seen from Figure 6 that the most likely set of models are the FN, RW, PL and GM plus VW models. It is worthwhile to notice that the VW only model is more likely than the FN, RW, PL and GM plus HW models for all components, especially for the vertical component. This not only may be result of the higher white noise amplitudes and the shortness of the time series as pointed out by Williams and Willis (2006), but also demonstrates the importance of considering the formal errors output by the GPS data processing software. To further investigate which model is the most likely model, we regarded the FN+VW model as the null hypothesis and compared the δ ML based on the criteria a 95^{th} percentile δ ML of around 3. As a result, the only accepted model is the GM+VW model. Although the statistic analysis indicates the preferred model is the GM+VW model, we prefer the flicker noise plus variable white noise (FN+VW) based on the following reasons. Firstly, the previous studies have shown that the colored noise in CGPS time series is consistent with flicker noise (Zhang *et al.*, 1997; Mao *et at.*, 1999; Williams *et al.*, 2004). Secondly the spread of the estimated cross-over frequency is large, which should be a constant in reality (see Williams and Willis (2006) for the detailed explanation). In addition, MLE greatly increases the computational time using the GM+VW model. For example, estimating the noise parameters of the HKFN site for the FN+VW model took 48 minutes for all three components, while estimating the noise parameters for the GM+VW model took 12.5 hours. Lastly, the estimated velocity uncertainties using the FN+VW model are larger by the average factor of 2.1 than the GM+VW model for our time series. Therefore, the flicker noise model is slightly more conservative.

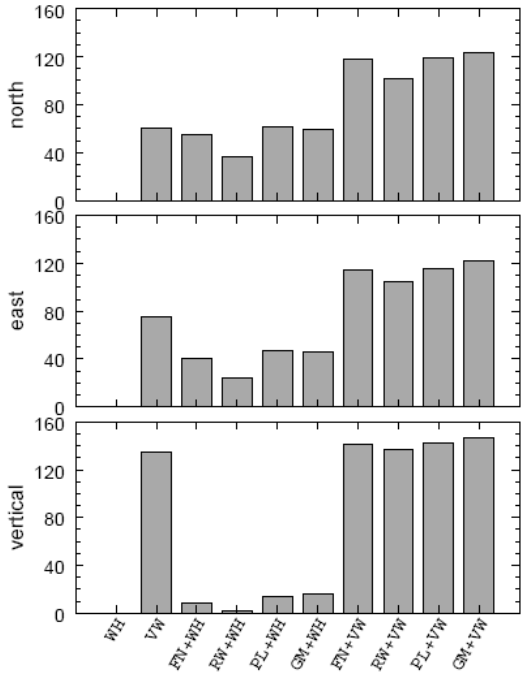

Figure 6. Average δ ML values for each noise model of all 12 sites with respect to the null hypothesis model that the noise consists of white noise only.

Table 2 lists the noise parameter estimates for the filtered time series based on the FN+VW model and the WRMS scatters also are shown. It can be seen from figure 6 and table 2 that the scaled formal errors adequately represent the white noise component of the time-series. The mean scaling factors are 0.35±0.04, 0.28±0.05 and 0.40±0.04 for the north, east, and vertical components, which are equal to the mean white noise amplitudes of 1.0±0.1 mm, 1.1 ±0.2 mm and 4.3±0.4 mm. The corresponding flicker noise values are 1.46±0.50 mm/yr$^{1/4}$, 1.92±0.77 mm/yr$^{1/4}$ and 2.89±0.87 mm/yr$^{1/4}$. For comparison, we also calculated the noise parameters for the CME time series based on the FN+HW model. The estimated white noise amplitudes are 1.32±0.08 mm, 2.50±0.10 mm and 3.72±0.21 mm; the corresponding flicker noise amplitudes are 8.24±0.30 mm/yr$^{1/4}$, 11.89±0.45 mm/yr$^{1/4}$ and 20.62±0.84 mm/yr$^{1/4}$. These results indicate that spatial filtering greatly reduces the flicker noise amplitudes, while the amplitude noise amplitudes are not significantly changed. This also can explain the failure of the MLE to estimate the flicker noise coefficients for some short filtered time series since the flicker noise is masked by the lager white noise for these short filtered time series.

Table 2. Variable white noise and flicker noise amplitude estimates for the north, east and vertical components of the filtered position time series.

Site	Span (year)	Variable white noise factor			Flicker noise(mm/yr$^{1/4}$)			WRMS(mm)		
		N	E	U	N	E	U	N	E	U
HKFN	6.7	0.34	0.25	0.36	1.14	2.43	2.98	1.03	1.25	3.67
HKKT	6.7	0.33	0.23	0.37	1.26	1.80	3.08	0.95	1.04	3.26
HKLT	6.7	0.30	0.26	0.37	1.89	2.03	4.27	0.95	1.17	3.36
HKMW	3.1	0.34	0.25	0.40	1.24	1.52	0.00	0.85	0.95	2.92
HKNP	3.1	0.45	0.40	0.49	1.96	2.91	0.00	1.19	1.56	3.70
HKOH	3.2	0.39	0.32	0.45	2.18	3.77	2.91	1.13	1.50	3.83
HKPC	2.9	0.35	0.26	0.36	0.96	1.03	0.00	0.85	0.94	2.82
HKSC	4.9	0.32	0.24	0.36	1.33	1.42	2.40	0.93	0.98	3.44
HKSL	6.7	0.32	0.24	0.37	1.28	1.62	3.80	0.92	1.05	3.50

HKSS	3.2	0.42	0.32	0.43	2.31	1.70	1.56	1.24	1.21	3.35
HKST	6.7	0.33	0.25	0.41	1.20	1.62	2.15	0.92	1.09	3.43
HKWS	3.2	0.37	0.31	0.41	0.72	1.22	0.00	0.88	1.13	3.14
Mean		0.35 ±0.04	0.28 ±0.05	0.40 ±0.04	1.46 ±0.50	1.92 ±0.77	2.89 ±0.87	0.99 ±0.13	1.16 ±0.20	3.37 ±0.30

The underlined items represent the MLE software failing to estimate the flicker noise coefficient.

3.3 Station Velocities and Their Uncertainty

Velocity estimates and their uncertainties of the filtered time series are given in Table 3 for the FN+VW model, with respect to the ITRF2005. The scale column indicates the value the velocity uncertainties need to be scaled by to take into account the presence of colored noise, if the velocity and its uncertainty had been estimated using the VW only model, that is weighted least squares. It can be seen from table 3 that velocity uncertainties for FN+VW model are about 2-6 times larger than the uncertainties for the VW only model. The horizontal velocity uncertainties for about 6.7 years time series are less than 0.2 mm/yr, and less than 0.5 mm/yr for about 3 years; the vertical uncertainties are also within 0.5 mm/yr. we also plotted the horizontal velocities relative to the station HKFN in order to give insight into the velocity inconsistency (Figure 7). The relative horizontal velocity map shows that the relative horizontal velocities have an increasing trend toward the southeast direction as a whole. The sites HKNP and HKOH show significantly different velocity magnitudes and directions. The HKNP relative velocity is 1.44±0.32 mm/yr oriented S30±15° W, and the HKOH relative velocity is 1.17±0.42 mm/y oriented S48±20° W. The velocity inconsistency indicates some local fault activities in our study region. However, as indicated, the velocity uncertainties are a little large so that we can not confirmatively declare the velocity differences. It will take considerably longer time series to better assess the local velocity differences.

Table 3. Estimated ITRF2005 velocities and their uncertainties (1 σ) based on the flicker noise plus variable white noise model.

Site	Velocity, mm/yr			Scale		
	N	E	U	N	E	U
HKFN	-13.63±0.08	31.15±0.16	1.49±0.23	3.26	5.23	2.52
HKKT	-14.22±0.09	31.19±0.12	0.77±0.23	3.76	4.63	2.83
HKLT	-14.00±0.13	31.73±0.14	0.91±0.31	5.26	4.56	3.60
HKMW	-14.27±0.18	31.70±0.22	0.54±0.38	4.06	4.35	2.55
HKNP	-14.87±0.28	30.42±0.41	0.65±0.48	4.38	4.84	2.55
HKOH	-14.41±0.29	30.28±0.49	0.22±0.46	5.44	6.80	2.46
HKPC	-13.56±0.15	31.21±0.16	1.99±0.38	3.25	3.14	2.55
HKSC	-13.61±0.16	32.13±0.17	0.02±0.36	3.10	3.12	1.88
HKSL	-13.93±0.09	31.97±0.12	0.44±0.29	3.91	4.20	3.16
HKSS	-13.87±0.30	31.31±0.23	-0.60±0.27	5.51	4.16	1.87
HKST	-13.92±0.10	32.07±0.13	0.94±0.20	3.60	4.00	2.05
HKWS	-14.20±0.11	31.81±0.18	-0.26±0.36	2.49	3.08	2.55

The scale column indicates the value the velocity uncertainties need to be scaled by to take into account the presence of colored noise, if the velocity and its uncertainty had been estimated using the VW only model, that is weighted least squares.

The underlined items represent the MLE software failing to estimate the flicker noise coefficient. The corresponding velocity and its uncertainty had been estimated using the only variable white noise

mode, that is weighted least squares. And then the velocity uncertainties (the underlined items) are scaled by the estimated average factors.

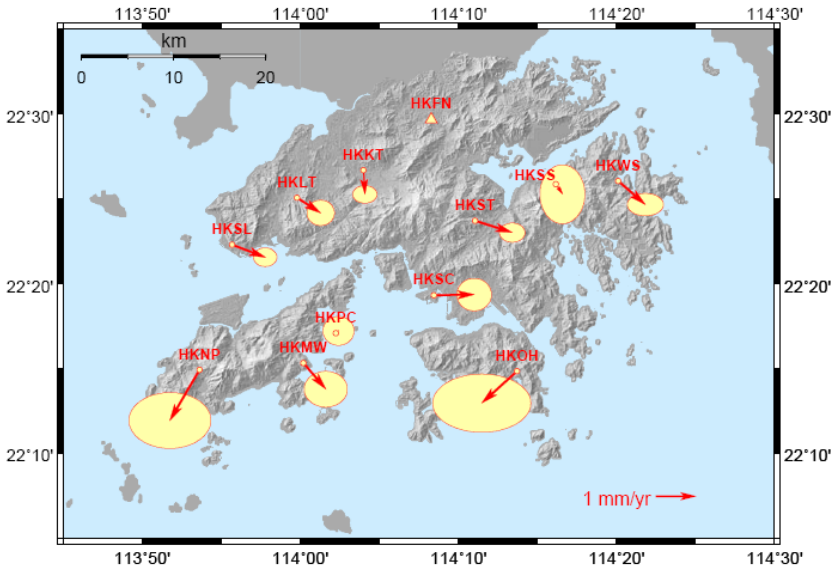

Figure 7. Map showing station horizontal velocities relative to station HKFN (triangle) their uncertainties at 95% confidence level based on the flicker noise plus variable white noise model.

3.4 Local Seasonal Variations

As mentioned in section 3, the spectral analysis suggests that the annual and semiannual signals exist for all three coordinate components in the filtered time series (see Figure 3). The estimated annual and semiannual amplitudes are given in Table 4 based on the flicker noise plus variable white noise model, respectively. It is seen from results in Table 4 that the amplitudes of the annual signal in all three coordinate components are more significant than the semiannual amplitudes. The annual and semi-annual signals in the height components are much stronger than those in the horizontal components. The horizontal semiannual signals are relatively insignificant. The annual amplitudes are up to 0.7 mm, 1.5 mm and 2.2 mm for north, east and vertical components, respectively. The corresponding semiannual amplitudes are up to 0.3mm, 0.4 mm and 0.9 mm. These local seasonal variations have the same order magnitude with the common mode errors (see section 3.1), especially for the annual variations, which suggests that the local geophysical derived variations or site-related modeling errors play an important role in the seasonal variations of the GPS coordinate time series.

Table 4. Estimated annual and semiannual amplitudes and their uncertainties (1 σ) based on the flicker noise plus variable white noise model.

Site	Annual amplitude (mm)			Semiannual amplitude (mm)		
	N	E	U	N	E	U
HKFN	0.41±0.07	0.86±0.13	0.93±0.19	0.18±0.05	0.17±0.09	0.13±0.16
HKKT	0.67±0.07	1.14±0.10	0.50±0.19	0.19±0.05	0.38±0.07	0.25±0.15
HKLT	0.30±0.10	0.49±0.11	2.24±0.25	0.17±0.07	0.29±0.08	0.88±0.19
HKMW	0.15±0.11	0.14±0.13	1.38±0.23	0.03±0.08	0.10±0.09	0.11±0.11
HKNP	0.46±0.16	0.98±0.23	0.66±0.28	0.18±0.12	0.44±0.17	0.37±0.24
HKOH	0.67±0.17	0.62±0.29	1.05±0.29	0.23±0.12	0.24±0.20	0.39±0.23

HKPC	0.63±0.09	1.46±0.10	0.32±0.25	0.06±0.07	0.05±0.07	0.30±0.20
HKSC	0.34±0.09	0.76±0.10	0.29±0.19	0.12±0.06	0.15±0.07	0.24±0.16
HKSL	0.35±0.07	0.08±0.09	0.43±0.23	0.17±0.05	0.17±0.07	0.72±0.17
HKSS	0.31±0.18	1.52±0.14	0.75±0.19	0.32±0.13	0.30±0.10	0.46±0.17
HKST	0.33±0.07	0.22±0.09	0.44±0.16	0.07±0.05	0.20±0.07	0.31±0.14
HKWS	0.21±0.07	0.56±0.11	0.73±0.25	0.11±0.06	0.12±0.08	0.66±0.19

The underlined items represent the MLE software failing to estimate the flicker noise coefficient. The corresponding annual parameters and their uncertainties had been estimated using the only variable white noise mode, that is weighted least squares. And then the annual and semiannual amplitude uncertainties are scaled by the estimated average factors.

It should be noticed that the daily residual scatters of all filtered time series also show strong seasonal characteristics. For example, the daily residuals of the filtered time series at site HKFN (Figure 8) clearly demonstrate that the daily residual scatters are larger during the summer than during the winter. This is likely caused by error sources that are temperature-dependent, such as local tropospheric perturbation, antenna thermal noise, and monument instability.

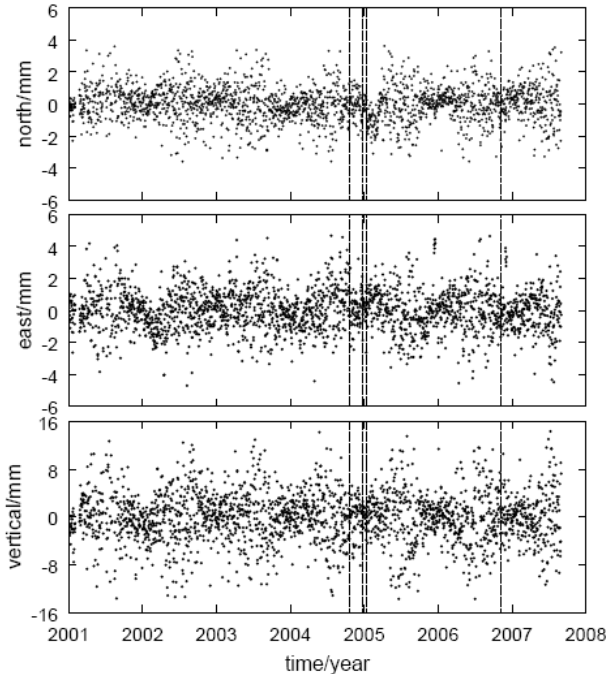

Figure 8. Daily residuals of the filtered time series at site HKFN after the model parameters have been removed. Vertical dashed lines indicate epochs at which an offset was introduced. For clarity the error bars are not shown. The WRMS of the residuals are 1.0mm, 1.2mm and 3.7mm for north, east and vertical components, respectively.

4. CONCLUSIONS

In this paper, six-year continuous GPS observations of 12 GPS stations from the Hong Kong local dense GPS network have been analysed to assess the consistency of daily position time series. The following conclusions can be drawn from the study.

Common mode errors are a dominant error source in the daily GPS solutions and they have strong seasonal signals in all the three coordinate components. Common mode errors account

for 93.9%, 94.2%, and 84.6% of the total non-linear variances of daily position time series for the north, east, and vertical components, respectively. The higher-order ionospheric effects are the prominent factor of impacting on the GPS coordinates in our studying area.

The colored noise of the daily position time series is drastically reduced by spatial filtering. The MLE analysis suggests that a combination of flicker noise and variable white noise is an appropriate stochastic model for all three components of the filtered position time series. The velocity uncertainties for FN+VW model are about 2-6 times larger than the uncertainties for the VW only model. The horizontal velocity uncertainties for about 6.7 years time series are less than 0.2 mm/yr, and less than 0.5 mm/yr for about 3 years; the vertical uncertainties are also within 0.5 mm/yr. Relative horizontal and vertical velocity inconsistencies at sites within 50 km of Hong Kong are both on the order of 2 mm/yr. Although we have chosen flicker noise as the colored noise model, we can not exclude first-order Markov or power-law noise as an optional model.

Local seasonal signatures in all three coordinate components of the filtered coordinate time series have been detected. The annual amplitudes are up to 0.7 mm, 1.5 mm and 2.2 mm for north, east and vertical components, respectively. The corresponding semiannual amplitudes are up to 0.3 mm, 0.4 mm and 0.9 mm. These local seasonal variations have the same order magnitude with the common mode errors, especially for the annual variations. The residual scatters of the filtered time series also show strong seasonal characteristics.

The potential geophysical variations and the modeling errors that cause these common mode and local variations of the coordinate time series are necessary to further investigate, especially the higher-order ionospheric effects. It is also necessary to identify the local fault activity in our study region especially by increasing the length of the GPS data sets.

Acknowledgements. We gratefully acknowledge Simon D. P. Williams who kindly provided his maximum likelihood estimation software. Thanks SIO for the freely available global GPS data and solutions and MIT for the GAMIT/GLOBK software. The figures in this paper were generated using the public domain Generic Mapping Tools (GMT) software (Wessel and Smith, 1995). The work was supported by the Research Grants Council of the Hong Kong Special Administrative Region (Grant No.: PolyU5157/05E and PolyU5161/06E). The first author is grateful to the Hong Kong Polytechnic University for providing the Ph.D. scholarship for the research (RGLV).

REFERENCES

Altamimi, Z., X. Collilieux, J. Legrand, B. Garayt, and C. Boucher (2007) ITRF2005: A new release of the International Terrestrial Reference Frame based on time series of station positions and Earth Orientation Parameters, *Journal Geophysical Research*, 112, B09401, doi:10.1029/2007JB004949.

Beavan, J. (2005) Noise properties of continuous GPS data from concrete pillar geodetic monuments in New Zealand and comparison with data from U.S. deep drilled braced monuments, *Journal Geophysical Research*, 110, B08410, doi:10.1029/2005JB003642.

Boehm, J., R. Heinkelmann and H. Schuh (2007) Short Note: A global model of pressure and temperature for geodetic applications, *Journal of Geodesy*, in press.

Boehm, J., A. Niell, P. Tregoning, and H. Schuh (2006) Global Mapping Function (GMF): A new empirical mapping function based on numerical weather model data, *Geophysical Research Letter*, 33, L07304, doi: 10.1029/2005GL025546.

Chen W., S. Gao, C. Hu, Y. Chen and X. Ding (2007) Effects of ionospheric disturbances on GPS observation in low latitude area, *GPS Solutions*, Online, doi:10.1007/s10291-007-0062-z.

Dong, D., T. A. Herring, and R. W. King (1998), Estimating regional deformation from a combination of space and terrestrial geodetic data, *Journal of Geodesy*, 72, 200– 214.

Dong, D., P. Fang, Y. Bock, M. K. Cheng, and S. Miyazaki (2002) Anatomy of apparent seasonal variations from GPS-derived site position time series, *Journal Geophysical Research*, 107(B4), 2075, doi:10.1029/2001JB000573.

Dong, D., P. Fang, Y. Bock, F. Webb, L. Prawirodirdjo, S. Kedar, and P. Jamason (2006) Spatiotemporal filtering using principal component analysis and Karhunen-Loeve expansion approaches for regional GPS network analysis, *Journal Geophysical Research*, 111, B03405, doi:10.1029/2005JB003806.

Fritsche, M., R. Dietrich, C. Knofel, A. Rulke, S. Vey, M. Rothacher, and P. Steigenberger (2005) Impact of higher-order ionospheric terms on GPS estimates, *Geophysical Research Letter*, 32, L23311, doi:10.1029/2005GL024342.

Herring, T. A., R. W. King, and S. C. McClusky (2006a) *GAMIT Reference Manual: GPS Analysis at MIT version 10.3*, Mass. Inst. of Technol., Cambridge.

Herring, T. A., R. W. King, and S. C. McClusky (2006b) *GLOBK Reference Manual: Global Kalman filter VLBI and GPS analysis program version 10.3*, Mass. Inst. of Technol., Cambridge.

Hill, E. M., and G. Blewitt (2006) Testing for fault activity at Yucca Mountain, Nevada, using independent GPS results from the BARGEN network, *Geophysical Research Letter*, 33, L14302, doi:10.1029/2006GL026140.

Kedar, S., G. A. Hajj, B. D. Wilson, and M. B. Heflin (2003) The effect of the second order GPS ionospheric correction on receiver positions, *Geophysical Research Letter*, 30(16), 1829, doi:10.1029/2003GL017639.

Kreemer, C., W.E. Holt, and A.J. Haines (2003) An integrated global model of present-day plate motions and plate boundary deformation, *Geophysical Journal International*, 154, 8-34.

Langbein J (2004) Noise in two-color electronic distance meter measurements revisited. *Journal Geophysical Research*, 109(B4):B04406. DOI 10.1029/2003JB002819.

Lidberg M, Johansson JM, Scherneck H-G, Davis JL (2007) An improved and extended GPS-derived 3D velocity field of the glacial isostatic adjustment (GIA) in Fennoscandia. *Journal of Geodesy*, 81(3):213–230.

Mao, A., C. G. Harrison, and T. H. Dixon (1999) Noise in GPS time series, *Journal Geophysical Research*, 104, 2797– 2816.

McCarthy, D. D., and G. Petit (Eds.) (2004) *IERS conventions (2003)*, IERS Tech. Note 32, Verl. des Bundesamtes für Kartogr. und Geod., Frankfurt am Main, Germany.

Nikolaidis, R. (2002) Observation of geodetic and seismic deformation with the Global Positioning System, *Ph.D. thesis*, Univ. of Calif., San Diego.

Penna, N. T., M. A. King, and M. P. Stewart (2007) GPS height time series: Short-period origins of spurious long-period signals, *Journal Geophysical Research*, 112, B02402, doi:10.1029/2005JB004047.

Prawirodirdjo, L., and Y. Bock (2004) Instantaneous global plate motion mode from 12 years of continuous GPS observations, *Journal Geophysical Research*, 109, B08405, doi:10.1029/2003JB002944.

Press WH, Teukolsky SA, Vetterling WT, Flannery BP (2001) *Numerical recipes in Fortran 77: the art of scientific computing* (2nd edn). Vol. 1 of Fortran numerical recipes, Cambridge University Press, Cambridge, pp 569–577.

Wdowinski, S., Y. Bock, J. Zhang, P. Fang, and J. Genrich (1997) Southern California permanent GPS geodetic array: Spatial filtering of daily positions for estimating coseismic and postseismic displacements induced by the 1992 Landers earthquake, *Journal Geophysical Research*, 102, 18,057– 18,070.

Wessel, P., andW. H. F. Smith (1995) New version of the Generic Mapping Tools released, *Eos Trans*. AGU, 76, 329.

Williams, S. D. P., Offsets in Global Positioning System time series (2003) *Journal Geophysical Research*, 108(B6), 2310, doi:10.1029/2002JB002156.

Williams, S. D. P., Y. Bock, P. Fang, P. Jamason, R. M. Nikolaidis, L. Prawirodirdjo, M. Miller, and D. J. Johnson (2004) Error analysis of continuous GPS position time series, *Journal Geophysical Research*, 109, B03412, doi:10.1029/2003JB002741.

Williams, S. D. P., P. Willis (2006) Error Analysis of Weekly Station Coordinates in the DORIS Network, *Journal of Geodesy*, 80 (8-11):525-539, DOI: 10.1007/s00190-006-0056-6

Zhang, J. (1996) Continuous GPS measurements of crustal deformation in southern California, *Ph.D. dissertation*, Univ. of Calif., San Diego.

Zhang J, Bock Y, Johnson H, Fang P, Genrich JF,Williams S, Wdowinski S, Behr J (1997) Southern California Permanent GPS Geodetic Array: error analysis of daily position estimates and site velocities. *Journal Geophysical Research*, 102(B8):18035–18055.